Origin of anisotropy and metallic behavior in delafossite $PdCoO_2$

Khuong P. Ong,[1] Jia Zhang,[1] John S. Tse,[2] and Ping Wu[1,*]
[1]*Institute of High Performance Computing, 1 Fusionopolis Way, No. 16-16 Connexis, 138632, Singapore*
[2]*Department of Physics and Engineering Physics, University of Saskatchewan, 116 Science Place, Saskatoon, Saskatchewan, Canada S7N 0K4*

(Received 17 September 2009; revised manuscript received 2 February 2010; published 16 March 2010)

The electronic structure of $PdCoO_2$ has been studied using the full potential linearized augmented plane wave (FP-LAPW) method employing the Perdew-Burke-Ernzerhof generalized-gradient approximations. The role of valence Pd and Co orbitals to the electrical conduction in $PdCoO_2$ has been analyzed in detail. Based on the electronic structure and electron density distribution, causes for the conducting behavior of the Pd layer and insulating property of CoO_2 layer have been identified. The present results support the proposal that anisotropy in the conductivity behavior can be attributed to metallic interactions between hybridized orbitals derived from mixing of Pd $4d_{z^2}$, $4d_{x^2-y^2}$, and $4d_{xy}$ orbitals. However, a small contribution from Pd-5*s* orbital located at adjunct sites in the ***ab*** plane at the Fermi level was also found. In contrast, the conductivity in the ***c***-direction is limited by the antibonding Pd-O states and the insulating state of CoO_2 layer. Good agreement is obtained for the calculated and observed Co-L_2-L_3 x-ray absorption spectrum confirming only very small contribution of Co density of states at the Fermi level.

DOI: 10.1103/PhysRevB.81.115120 PACS number(s): 71.20.−b, 71.18.+y, 71.15.Mb, 72.15.−v

I. INTRODUCTION

Delafossite oxides (ABO_2) with alternate triangular O-A-O and octahedral BO_6 layers stack along the ***c*** axis,[1,2] have attracted much attention due to their novel physical properties such as frustrated antiferromagnetic, multiferroics properties,[3–5] which can be explored for using as quantum electromagnets. Some delafossites, e.g., $CuAlO_2$,[6,7] $CuGaO_2$,[8] $CuInO_2$,[9] have wide optical band gaps (>3 eV) that is advantageous in many important technological applications including flat panel displays, solar energy capture, and optoelectronic devices. Other delafossite oxides such as $PdCoO_2$, $PdRhO_2$, $PdCrO_2$, $PtCoO_2$, and $PtCrO_2$ have also attracted much interest due to their very high electrical conductivity.[10] Specifically, they can be used as a conductor in oxidizing environment especially as a current collector in solid oxide fuel cells. Among the metallic delafossite oxides, it was reported that $PdCoO_2$ is paramagnetic and possesses the lowest resistivity at the room temperature.[10,11] Electrical measurements also revealed a highly anisotropic electrical resistivity, which is substantially higher along the ***c***-axis than in the perpendicular plane.[11] The metallic nature of this compound has been interpreted as the result of overlap between hybridized Pd-$4d_{z^2}$-5*s* states.[12] Moreover, ^{59}Co-NMR (nuclear magnetic resonance) measurements,[13] resonant photoemission studies (RPES), resonant inverse photoemission studies (IREPS),[14] and X-ray absorption spectroscopy (XAS)[12] all indicate low[13] or very low[12,14] density of states at Fermi level (E_F) at the Co sites. The main contribution to the density of states (DOS) at the Fermi level is derived from Pd-4*d*.[12,14] XAS experiment[12] further revealed that the electronic state of Co and Pd in $PdCoO_2$ is trivalent and monovalent, respectively. Finally, a specific heat measurement[12] supported the *s-d* hybridized character of conduction electrons in $PdCoO_2$.

Theoretical studies have been performed by Okabe *et al.*,[15] Seshadri *et al.*,[16] and Eyert *et al.*[17] in order to explain the nature of the metal-metal bonding and electronic properties of $PdCoO_2$. According to Okabe *et al.*,[15] the density of states at the Fermi level (E_F) mainly originated from the Pd-4*d* states with small contributions from Co-3*d* and O-2*p* states. Band structure calculations by Seshadri *et al.*,[16] revealed a dominant contribution from Pd-$4d_{z^2}$ at the Fermi level while the DOS calculation by Eyert *et al.*,[17] showed a somewhat higher contribution of Pd-d_{xy} and $d_{x^2-y^2}$ states. The *s-d* hybridized character of conduction electrons as suggested by a specific heat measurement[12] has not been mentioned and the cause and anisotropy of the metallic behavior of $PdCoO_2$ have not been discussed in detail by previous theoretical works. In this paper, the apparent inconsistency between the theoretical results and particularly, the origin of the anisotropy in the electrical conductivity are examined. To this end, the electronic structure of $PdCoO_2$ was calculated with the density-functional theory (DFT) by applying the full potential linearized augmented plane wave (FP-LAPW) method employing the generalized gradient approximation (GGA). The mechanism of the strong anisotropy on the electrical conductivity is explained on the basis of the characters of the Pd and Co orbitals near the Fermi level. The bonding and role of the atomic orbitals is characterized unambiguously from analysis of the electron band structures, Fermi surface and electron density maps. Calculations of the x-ray absorption spectra (XAS) of $PdCoO_2$ were performed. The good agreement with experiment supports the accuracy of the present calculations.

II. COMPUTATIONAL DETAILS

At low temperature, $PdCoO_2$ was found to be weakly paramagnetic with a magnetic susceptibility of 5×10^{-3} emu/mol.[11] At higher temperature, the magnetic susceptibility was found to diminish rapidly and at room temperature it becomes negligibly small.[11] Therefore, it is reasonable to perform the electronic structure calculations using

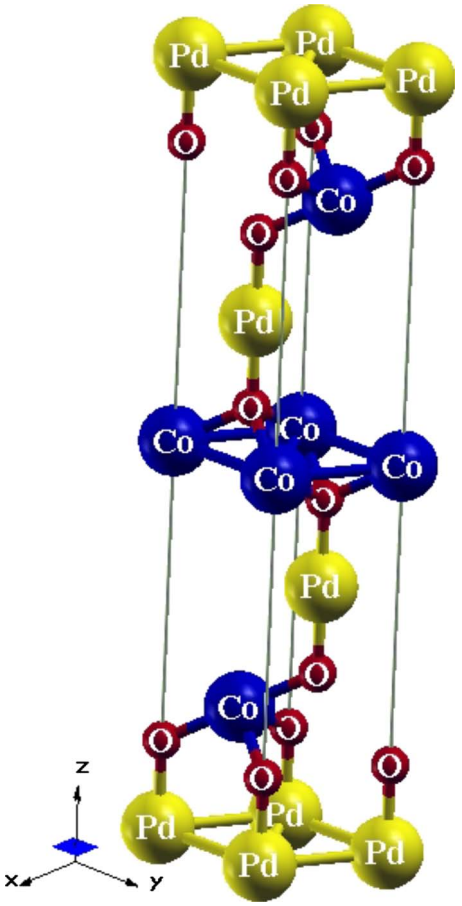

FIG. 1. (Color online) Crystal structure of $PdCoO_2$ Pd (yellow spheres), Co (blue sphere) and O (red spheres) occupy site 3*a* (0, 0, 0), site 3*b* (0, 0, 1/2), and site 6*c* (0, 0, 0.1125), respectively.

the spin-restricted formalism. As a check, it is found that the solution of a spin-unrestricted calculation converges to the spin-restricted result. All calculations were performed with the Wien2k software package.[18] This program computes the electronic structure of $PdCoO_2$ within the DFT utilizing full potential (linear) augmented plane wave+local orbitals (APW+lo) method and the Perdew-Burke-Ernzerhof generalized-gradient approximation (PBE-GGA).[19] $PdCoO_2$ crystallizes in the *R*-3*m* structure (space group No. 166) (see Fig. 1) with the Pd atoms situated at 3*a* (0, 0, 0), Co at 3*b* (0, 0, 0.5), and O at 6*c* (0, 0, $\pm u$) sites (u=0.1125). For the calculations, the lattice parameters of a=2.8317 Å and c =17.74 Å (in hexagonal setting) were taken from experiment[20] while the internal parameter u=0.1125 of the O atom was obtained from geometry optimization which is comparable with experiment value u=0.1112(8).[2] The very small difference between the predicted and experimental position of the oxygen atoms will make no difference to the results presented here. The electronic structure was calculated with the augmented plane wave+local orbital (APW +lo) basis set for **d** electrons and LAPW basis set for *s* and *p* electrons. The muffin tin radii (R_{MT}) for the atomic spheres were chosen as: 2.00 a.u, 1.85 a.u, 1.60 a.u for Pd, Co, and O, respectively. Inside the atomic spheres, partial waves were expanded up to l_{max}=10 with a plane wave cutoff $R_{MT}K_{max}$=8.0. The charge density was Fourier expanded up to G_{max}=16 Ry. The convergence of *k*-point sampling was checked up to 10 000 points in the full Brillouin zone. It is found that a *k*-mesh of 3000 *k*-points in the full Brillouin zone or 280 *k* points in the irreducible Brillouin zone (IBZ) was sufficiently accurate. In addition to the usual valence states, Pd-4*s*, 4*p*, 4*d*, 5*s*; Co-3*p*, 3*d*, 4*s*; and O-2*s*, 2*p* were treated as "semicore" states. The band dispersions are plotted along the high-symmetry points Γ(0,0,0), Z(1/2,1/2,1/2), F(1/2,1/2,0), and L(0,1/2,0) (Ref. 21) in the Brillouin zone. The calculated Fermi surface and electron density map are illustrated using the XCRYSDEN code.[22]

III. ORIGIN OF METALLIC BEHAVIOR AND ANISOTROPY OF $PdCoO_2$

The total/partial density of states (TDOS/PDOS) of $PdCoO_2$ are shown in Fig. 2. The theoretical results are in general agreement with previous calculations[15–17] and the Co^{59} NMR experiment.[13] It is found that the contribution from Co-*d* PDOS *at the Fermi level* is minor, which is in agreement with optical measurements[12,14] which suggested a low[13] to very low[12,14] Co-PDOS at the Fermi level. The calculated Pd-4*d* PDOS [Fig. 2(b)] shows Pd-$d_{x^2-y^2}$+d_{xy} and

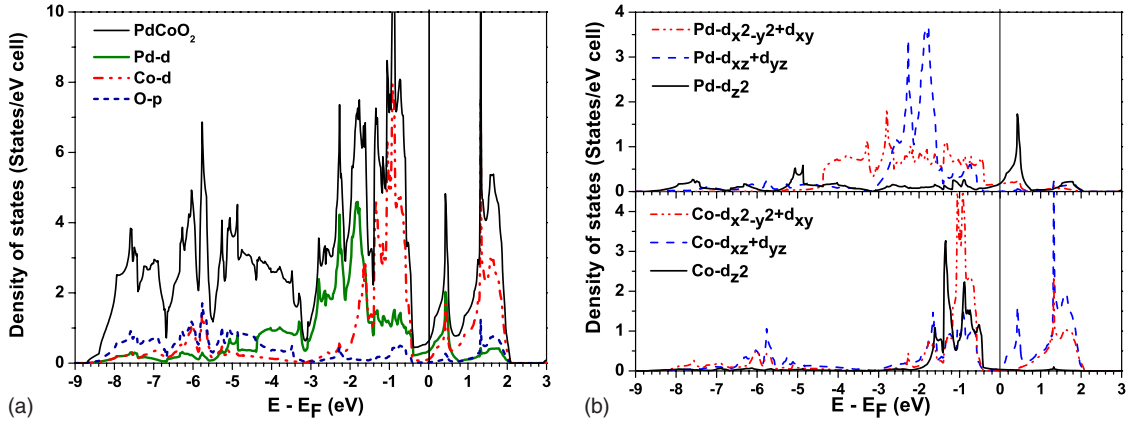

FIG. 2. (Color online) (a) Total/Partial Density of States (TDOS/PDOS) of $PdCoO_2$; (b) Partial Pd-4*d* DOS and Co-3*d* DOS of $PdCoO_2$

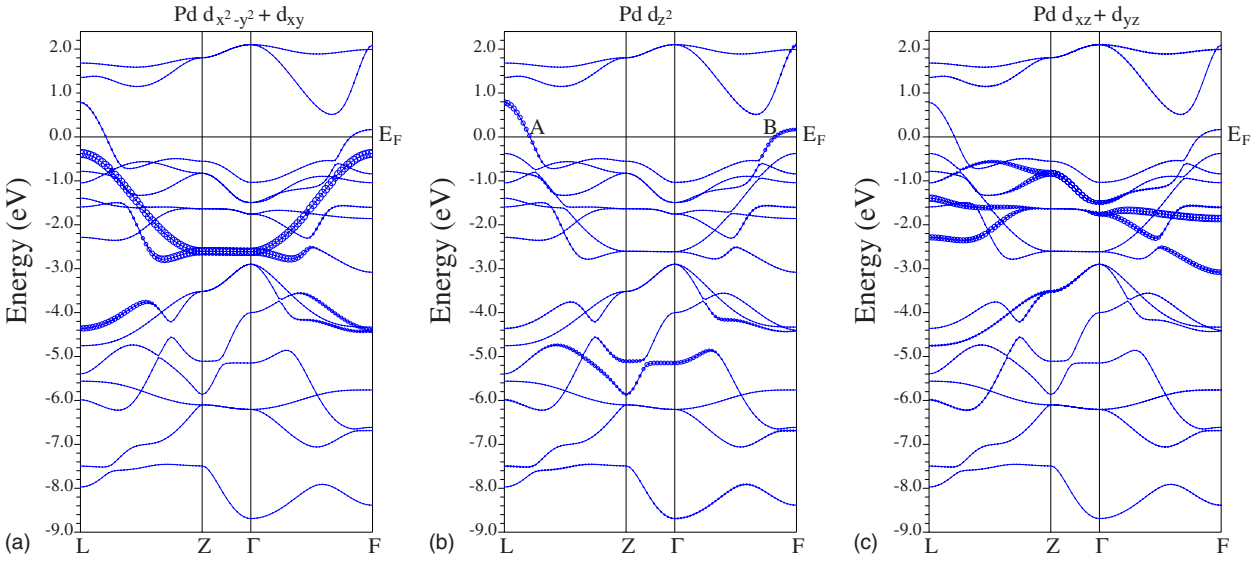

FIG. 3. (Color online) Band structure of (a) Pd-$d_{x^2-y^2}+d_{xy}$; (b) Pd-d_{z^2}; and (c) Pd $d_{xz}+d_{yz}$ states

Pd-d_{z^2} states contribute almost equally to the DOS at the Fermi level. This observation agrees with Ref. 17 but differs on a small difference on the relative contribution from the Pd-$d_{x^2-y^2}+d_{xy}$ and Pd-d_{z^2} states at the Fermi level. Moreover, as will be discussed below, we also found a small contribution from the Pd 5*s*. To identify which Pd-4*d* state plays the major role at the Fermi level, the electronic band structures projected into different Pd-4*d* orbitals were calculated (Fig. 3).

It is clear that there is only one electron band with larger Pd d_{z^2} character crosses the Fermi level. The Pd-$d_{x^2-y^2}+d_{xy}$ bands lying just below the Fermi level are rather broad extending from $(E\text{-}E_F)=-4.4$ to -0.38 eV. To illustrate these results, electron density map of the top valence band within the energy range from $(E\text{-}E_F)=-0.38$ to -0.25 eV in the $(10\bar{1}0)$ plane was calculated and plotted in Fig. 4(a).

The result clearly shows the characteristic of Pd-$4d_{x^2-y^2}$ and $4d_{xy}$ states (shown as the cross section of a large annular lobe in the $(10\bar{1}0)$ plane). Within the energy range from $(E\text{-}E_F)=-0.08$ eV to the Fermi level the electron density map of the top valence band in the $(10\bar{1}0)$ plane shows a stronger Pd d_{z^2} character with a slightly reduced annular lobe projected in the $(10\bar{1}0)$ plane [see Fig. 4(b)]. This observation indicates that near the Fermi level, the crystal orbital is composed of mixed Pd-d_{z^2}, $d_{x^2-y^2}+d_{xy}$ and perhaps some Pd-5*s* orbitals.

To verify this suggestion, the Pd electron density topology is analyzed further. From the band structure shown in Fig. 3, there is only one electronic band crossing the Fermi surface at A and B along L→Z and Γ→F, respectively. The charge density plot of the wave functions at A and B in the $(11\bar{2}0)$ plane are compared in Fig. 5. Gross features of the electron topology are very similar to Fig. 4. Electron density maps at A and B in the (0001) plane cutting through the Pd atoms were calculated and shown in the Fig. 6. It is surprising that the charge distributions at the Pd atoms in the A and B point projected in the ***ab*** plane resemble circles. Evidently, the spatial extend of the "circular" charge density around the Pd at point A is more extended (diffuse) than at point B. The circularlike charge distribution in the two-dimensional (2D) plane may suggest the participation of Pd 5*s* orbital.

However, inspection of the PDOS of the Pd atom at the Fermi level in Fig. 2 shows contribution from Pd $4d_{x^2-y^2}+4d_{xy}$ and $4d_{z^2}$ orbitals are of equal importance. Equal mixture of these orbitals can result in an apparent appearance of circular 2D distribution of electron density in the *xy* (***ab***) plane. Collecting all the information, a rather complex picture on the Pd hybridization starts to emerge. The Pd hybridization is best described as an admixture of Pd $4d_{x^2-y^2}$, $4d_{xy}$, $4d_{z^2}$ perhaps with a smaller contribution from Pd 5*s*. This is the only description which is consistent with both calculated charge distributions and the Pd PDOS. The spatially much

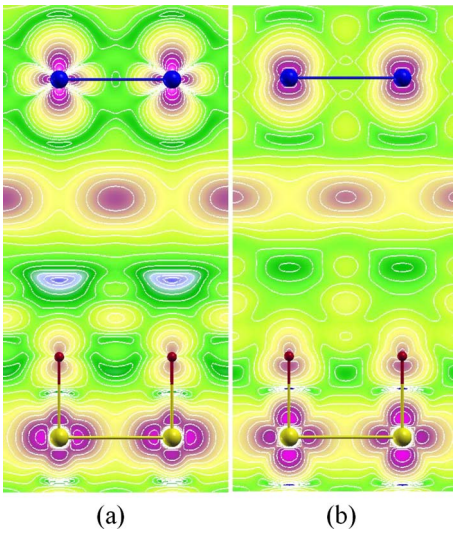

FIG. 4. (Color online) Electron density within the energy range: (a) from $(E\text{-}E_F)=-0.38$ to -0.25 eV and (b) from $(E\text{-}E_F)=-0.08$ eV to the Fermi level of $PdCoO_2$ in the $(10\bar{1}0)$ plane. The contour scale is the same as in Fig. 5

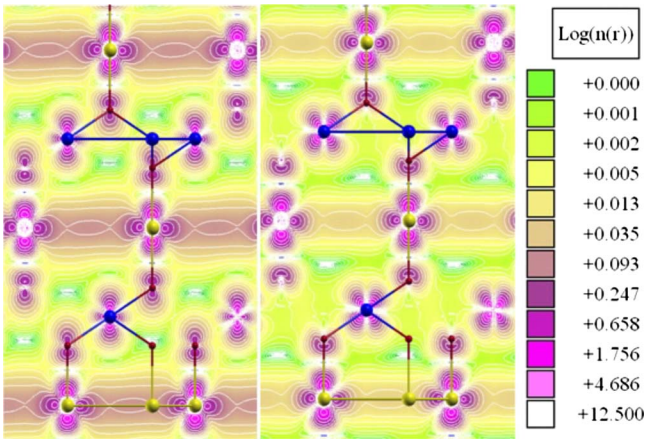

FIG. 5. (Color online) The charge density of the wave functions within the energy range from $(E\text{-}E_F)=-0.08$ eV to the Fermi level at: (a) A (0.69, 0, 0.3 a/c) $2\pi/a$ and (b) B (0.47, 0, 0.82 a/c) $2\pi/a$ point in the $(11\bar{2}0)$ plane.

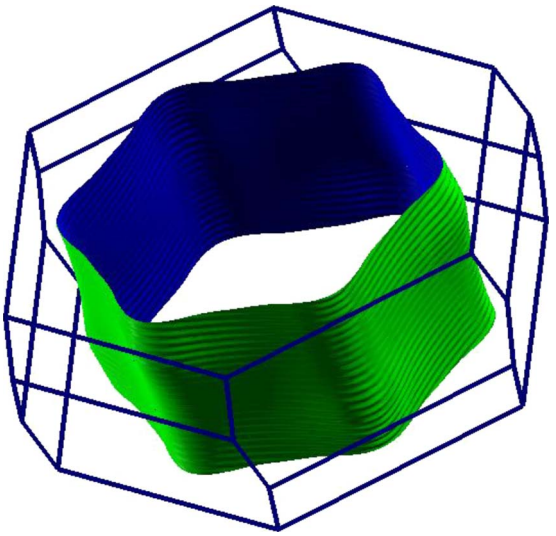

FIG. 7. (Color online) A three-dimensional plot for the Fermi surface of $PdCoO_2$

more diffuse Pd 5*s* orbitals are responsible for the extensive overlap (parallel to the *c*-axis in the $(10\bar{1}0)$ plane) between Pd atoms observed at the A point shown in Fig. 5. Since Pd-5*s* electron occupies the interstitial space, it is not displayed as prominent in the PDOS (Fig. 2) as the tighter Pd 4*d* in the atomic sphere region bound by the muffin-tin radius. This explanation highlights the possibility of Pd $4d_{z^2}$-5*s* hybridization suggested by Orgel.[23] In summary, the study of the charge density shows the overlaps between Pd in the ***ab*** plane is indeed more significant at point A than at B. Thus, the electrons at the Fermi level are more mobile in the Pd ***ab*** plane than along ***c***. This is manifested in the observed electrical conductivity anisotropy. The electron density maps shown in Fig. 5 and Fig. 6 shows an anti-Pd-O bonding character along the ***c***-direction perpendicular to the Pd plane in the energy interval $E\text{-}E_F \geq -0.38$ eV. This qualitative analysis indicates that there should be comparatively weaker electron transport along the *c*-axis from the Pd-layer to the Co-O layer within the energy range $E\text{-}E_F \geq -0.38$ eV. This is the additional reason for the anisotropy in the electric conductivity of $PdCoO_2$.

To further understand the observed anisotropy in electrical conductivity in $PdCoO_2$, the Fermi surface has been calculated and shown in Fig. 7. The topology of the Fermi surface, which is almost identical with the previous report,[17] is quasi two dimensional with wavelike surfaces due to the formation of holes at the L and F points. The small participation of

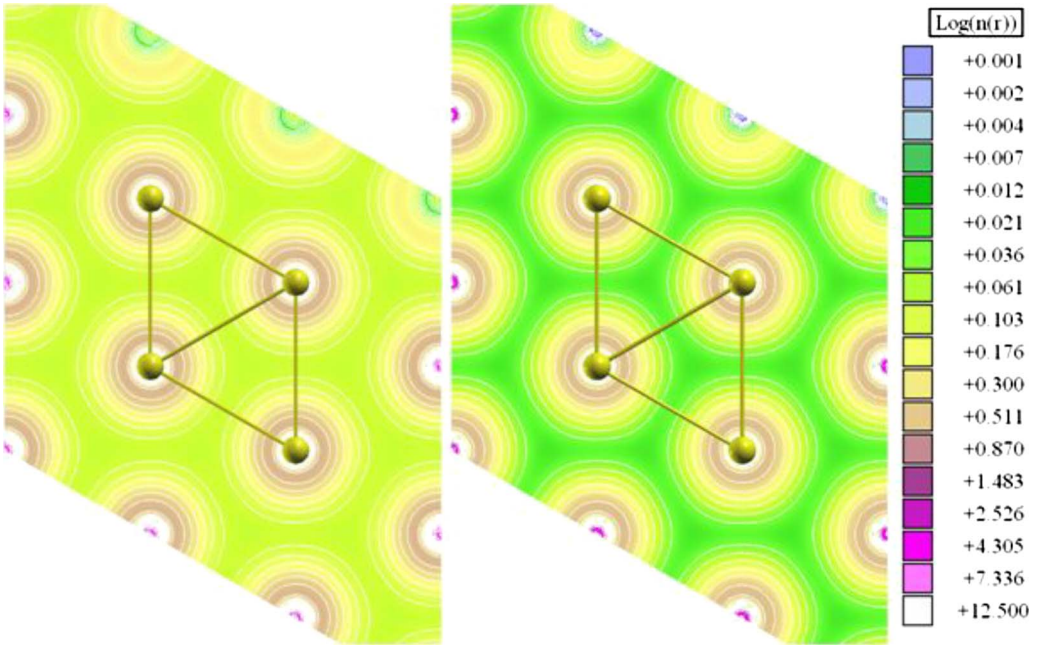

FIG. 6. (Color online) The charge density of the wave functions within the energy range from $(E\text{-}E_F)=-0.08$ eV to the Fermi level at (a) A (0.69, 0, 0.3 a/c) $2\pi/a$ and (b) B (0.47, 0, 0.82 a/c) $2\pi/a$ point in the (0001) plane cutting through the Pd atoms.

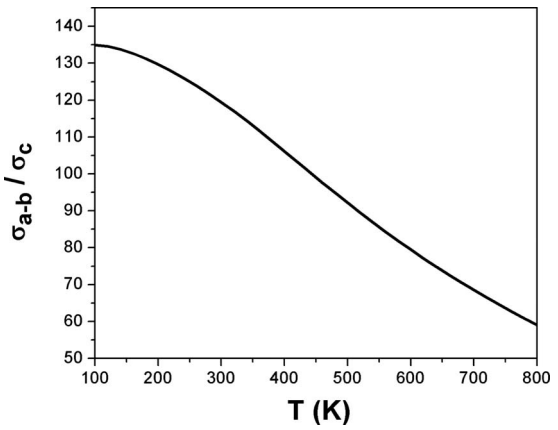

FIG. 8. Calculated temperature dependence of electrical conductivity ratio between the in-plane electrical conductivity ($\sigma_{a\text{-}b}$) and electrical conductivity along the ***c***-axis (σ_C)

Pd 5*s* does not alter features of the Fermi surface. A quasi-two-dimensional Fermi surface reflects high anisotropy in the electrical conductivity. From the electronic band structure (Fig. 3) the valence band crosses the Fermi level at point A and B. Near the vicinity of B and along the B→F direction, the electron band dispersion is very flat. Since the gradient of the band dispersion of the valence band crossing the Fermi level is smaller at B than at A, it is expected that the effective mass of the electron is heavier at B (v_B) than at A (v_A). This is confirmed by calculations showing that $v_A \sim 9.4 v_B$.

To quantify the strong anisotropy in conductivity, the electrical conductivity of $PdCoO_2$ in the plane ($\sigma_{a\text{-}b}$) and along the *c*-axis(σ_c) were calculated using the BoltzTraP code[24] based on the semiclassical Boltzmann theory with constant relaxation times. Convergence test shows that a *k*-mesh of 100 000 *k*-points for Brillouin zone integration is sufficiently accurate. The theoretical result for the ratio $\sigma_{a\text{-}b}/\sigma_c$ as a function of temperature is shown in Fig. 8. Over a wide temperature range from 100 to 800 K, the electrical conductivity in the plane is predicted to be higher than along the *c*-direction and the ratio of the conductivity decreases slightly at higher temperature.

Similar analysis of the electronic band and DOS were performed on the Co atoms. The Co-PDOS reveals contributions from Co-d_{z^2} and Co-$d_{xz}+d_{yz}$ in the valence band. There are some Co-$d_{xz}+d_{yz}$ characters in the valence band crosses the Fermi level at B (Fig. 9). In comparison to Pd, the participation of the Co orbitals is, however, very small. There is no direct Co-Pd interaction. Near the top of the Fermi level, the Co electrons mainly localized in the Co-O anti-bonding orbitals and with negligible overlap between them. In comparison to the Pd-(***ab***) plane, the lack of overlap inhibited electron delocalization and resulted in the poor electrical conductance in the Co-plane [see Fig. 4(b) and 5]. Therefore, the Co ***ab*** plane can be considered as an insulating layer.

To validate the quality of the electronic structure of $PdCoO_2$ obtained from the present calculation which suggests very low Co-DOS at the Fermi level, the x-ray absorption spectra of Co-2*p* with and without core-hole approximation were performed. For comparison, the experimental spectra[12] were shifted to align the main major peak Co-$2p_{3/2}$ (L_{III}) with the theoretical XAS. The result computed without a Co-core hole shown in Fig. 10 predicted a small peak at 3.1 eV which is 1 eV lower than the experimental peak. In comparison, using the core hole approximation with a super cell of $2\times2\times2$, the calculated Co-2*p* XAS spectrum shows a pronounced peak at 4.1 eV which is in good agreement with experiment. The good agreement between theory and experiment indicates the calculated DOS in the present study is reliable.

IV. SUMMARY

Detailed analyses of the electron band structure, electronic density of states and electron density distribution at the Fermi level have shown unambiguously that the electrical conductivity of $PdCoO_2$ originates from Pd layers sandwiched by alternating "*insulating*" CoO_2 layers perpendicu-

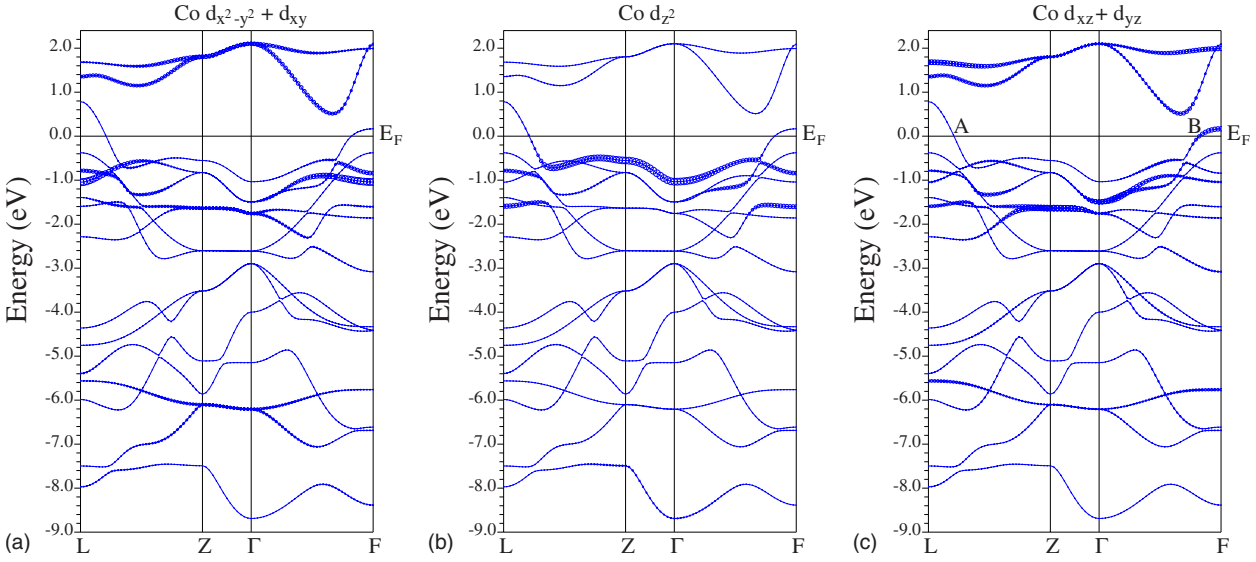

FIG. 9. (Color online) Band structure of (a) Co-$d_{x^2-y^2}+d_{xy}$; (b) Co-d_{z^2}; and (c) Co-$d_{xz}+d_{yz}$ states

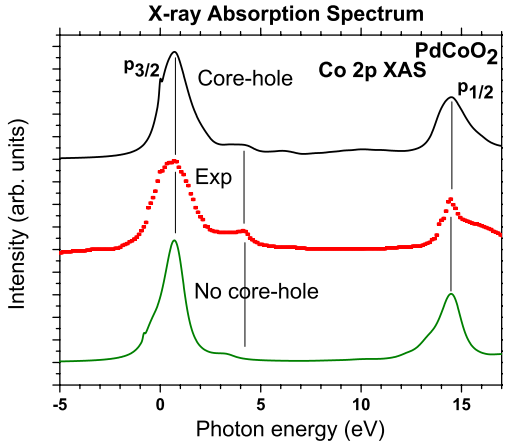

FIG. 10. (Color online) Calculated Co-2*p* x-ray absorption spectra of $PdCoO_2$ with and without core hole approximation. The red squares are experimental data reproduced from Ref. 12.

lar to the ***c*** axis. Overlaps between hybrid orbitals compose of Pd 4(d_{z^2}, $d_{x^2-y^2}$, d_{xy}) and 5*s* at the Fermi level resulted in delocalized metallic bonding and responsible for the electrical conductivity. The antibonding interactions between Pd and O along the *c* axis around the Fermi level leads to a very weak electrical conductance. The insulating characteristic of CoO_2 layer is confirmed. The results presented here are also applicable to rationalize the high-electrical conductivity anisotropy in the delafossite family.

ACKNOWLEDGMENT

Financial support from the Institute of High Performance Computing (IHPC) and Agency of Science, Technology, and Research (A*STAR) is gratefully acknowledged. K.P.O would like to thank Robert Laskowski and Peter Blaha for helpful discussions on the electron-core hole spectra of $PdCoO_2$.

*Corresponding author; wuping@ihpc.a-star.edu.sg

[1] R. D. Shannon, D. B. Rogers, and C. T. Prewitt, Inorg. Chem. **10**, 713 (1971).
[2] C. T. Prewitt, R. D. Shannon, and D. B. Rogers, Inorg. Chem. **10**, 719 (1971).
[3] T. Kimura, T. Goto, H. Shintani, K. Ishizaka, T. Arima, and K. Tokura, Nature (London) **426**, 55 (2003).
[4] N. Hur, S. Park, P. A. Sharma, J. S. Ahn, S. Guha, and S.-W. Cheong, Nature (London) **429**, 392 (2004).
[5] T. Lottermoser, T. Lonkai, U. Amann, D. Hohlwein, J. Ihringer, and M. Fiebig, Nature (London) **430**, 541 (2004).
[6] F. A. Benko and F. P. Koffyberg, J. Phys. Chem. Solids **45**, 57 (1984).
[7] H. Yanagi, S. Inoue, K. Ueda, H. Kawazoe, H. Hosono, and N. Hamada, J. Appl. Phys. **88**, 4159 (2000).
[8] K. Ueda, T. Hase, H. Yanagi, H. Kawazoe, H. Hosono, H. Ohta, M. Orita, and M. Hirano, J. Appl. Phys. **89**, 1790 (2001).
[9] H. Yanagi, T. Hase, S. Ibuki, K. Ueda, and H. Hosono, Appl. Phys. Lett. **78**, 1583 (2001).
[10] D. B. Rogers, R. D. Shannon, C. T. Prewitt, and J. L. Gillson, Inorg. Chem. **10**, 723 (1971).
[11] M. Tanaka, M. Hasegawa, and H. Takei, J. Phys. Soc. Jpn. **65**, 3973 (1996).
[12] M. Tanaka, M. Hasegawa, T. Higuchi, T. Tsukamoto, Y. Tezuka, S. Shin, and H. Takei, Physica B **245**, 157 (1998).
[13] M. Itoh, M. Mori, M. Tanaka, and H. Takei, Physica B **259-261**, 999 (1999).
[14] T. Higuchi, T. Tsukamoto, M. Tanaka, H. Ishii, K. Kanai, Y. Tezuka, S. Shin, and H. Takei, J. Electron Spectrosc. Relat. Phenom. **92**, 71 (1998); T. Higuchi, M. Hasegawa, M. Tanaka, H. Takei, S. Shin, and T. Tsukamoto, Jpn. J. Appl. Phys. **43**, 699 (2004).
[15] H. Okabe, M. Matoba, T. Kyomen, and M. Itoh, J. Appl. Phys. **93**, 7258 (2003).
[16] R. Seshadri, C. Felser, K. Thieme, and W. Tremel, Chem. Mater. **10**, 2189 (1998).
[17] V. Eyert, R. Fresard, and A. Maignan, Chem. Mater. **20**, 2370 (2008).
[18] P. Blaha, K. Schwarz, G. K. H. Madsen, D. Kvasnicka, and J. Luitz, *WIEN2k, An Augmented Plane Wave+Local Orbitals Program for Calculating Crystal Properties* (Karlheinz Schwarz, TU Vienna, Austria, 2009).
[19] J. P. Perdew, K. Burke, and M. Ernzerhof, Phys. Rev. Lett. **77**, 3865 (1996); **80**, 891 (1998).
[20] M. Tanaka, M. Hasegawa, and H. Takei, J. Cryst. Growth **173**, 440 (1997).
[21] C. J. Bradley and A. P. Cracknell, *The Mathematical of Symmetry in Solids* (Clarendon Press, Oxford, 1972).
[22] A. Kokalj, Comput. Mater. Sci. **28**, 155 (2003).
[23] A. J. Orgel, *An Introduction to Transition-Metal Chemistry: Ligand-Field Theory* (Wiley, New York, 1960).
[24] G. K. H. Madsen and D. J. Singh, Comput. Phys. Commun. **175**, 67 (2006).